Penetration depth study for a Sub-Surface MRI System

Supported by Kodak/CIS Innovative Graduate Student Grant

Christina Bray, Principal Investigator, Graduate Student
Tyler Lucero, Summer Intern
Joseph Hornak, Faculty Sponsor, Thesis Advisor
Chester F. Carlson Center for Imaging Science
Rochester Institute of Technology

Abstract

The materials used in organic light emitting diodes (OLED) and liquid crystal displays (LCD) are subject to deterioration in performance from moisture ingress, but little is known about the process. Nuclear magnetic resonance (NMR) and magnetic resonance imaging (MRI) modalities are well suited to study these display materials. We are exploring various designs for a sub-surface MRI system suitable for imaging these displays and other objects to a depth of 10 mm and greater in non-ferromagnetic proton-rich media. Using an innovative approach that leverages the post-acquisition subsystems of a commercial NMR spectrometer has dramatically reduced our development time and our research support costs. As shared in an earlier document, integration of our subsurface imaging *proof-of-concept* device with R.I.T.'s Bruker 300 MHz, DRX, 100 Watt spectrometer has had limiting consequences on our system's performance capability. This report will summarize the current imaging performance of our MRI application as well as share data that had been collected from a solids-enabled spectrometer. Indeed, our *proof-of-concept* device coupled with Xerox's high power (1000 Watt) spectrometer, did exhibit improved penetration depth performance as compared with the performance seen with our 300MHz host instrument.

Support Funding Received: $4,800.00

Funding Dates: June 1 through August 30, 2005.

Background

Early on in our investigations we were primarily interested in the geophysical application of non-invasive sub-surface detection and location of underground utilities using MRI. The gold standard imaging modality for sub-surface utility detection is ground penetrating radar (GPR). However, GPR has limitations for its usefulness and in such cases where the soils are saturated with water or have a high conductivity characteristic.[1] In the soil environments where GPR breaks down MRI would perform quite well, but more work was needed to understand the solution space for this imaging modality. To date, much work has been completed in understanding critical NMR imaging parameters.[2-4] In parallel to performing these mono-dispersed soil studies, we constructed a laboratory *proof-of-concept* sub-surface MRI system. We have obtained signal from several prototype iterations and have acquired several images using variations of a top-hat phantom[5] , as well as other non-symmetric targets. At the depths that we have been able to image with the College of Science, (COS) Bruker 300 MHz spectrometer, we have found that our prototype instrument is suitable for water ingress studies with OLED and LED displays. With the 300 MHz host spectrometer, we have obtained optimized signal acquisition parameters for our *proof-of-concept* device.[6] However, the host-system limitations have constrained the depth performance that we have been able to achieve.

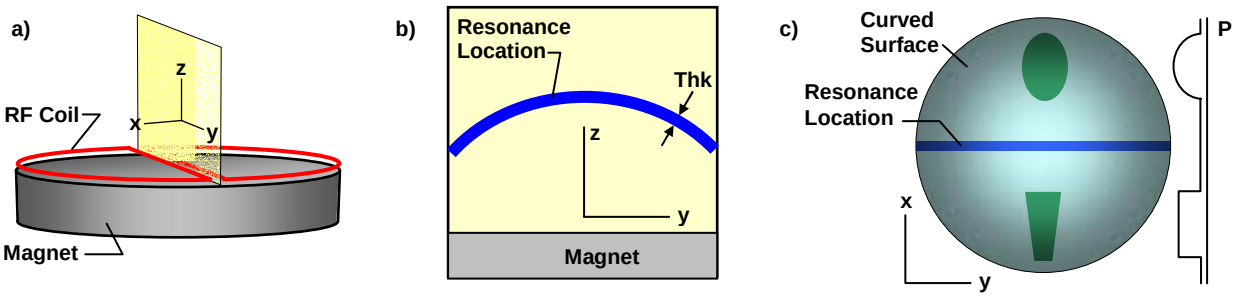

Fig. 1. Schematic representations of the a) MRI prototype apparatus, b) resonance location in the ZY plane, and projection of the signal in the resonance location as the RF coil is moved along X.

A schematic of our *Proof-of-concept* MRI device is shown in Figure 1.0. In this system, a permanent magnet source (Fig. 1a) produces a static field, B_o, along the Z axis and a butterfly coil[7] adjacent to the magnet surface produces a RF field, B_1. The resulting imaging sensitive region for this configuration is defined by a plane parallel to the Z axis and bisects the center of the RF coil. For an RF coil resonant at a frequency ν_o, B_o equals ν_o divided by the gyromagnetic ratio in a curved surface above the magnet. Due to the requirement that $B_1 \perp B_o$, spins are only excited in an arc above the magnet and RF coil, and in the XY plane (see Fig. 1b). The thickness (Thk) of the arc is determined by the bandwidth of the excitation RF pulses and the gradient in B_o. The NMR signal as a function of X location of the RF coil represents the projection of the NMR signal in the curved surface onto the projection axis, P, or Y-axis in this case. (See Fig. 1c.) Varying the orientation of the RF coil in the XY-plane will produce projections at angles ϕ about Z. This 2D imaging is similar to projection imaging[8] except the imaged surface is curved. Reconstruction of the image involves warping of the result of the inverse Radon transform[9] onto the curved surface.

To date, we have completed the characterization of various components comprising the device shown in schematic form in Fig. 1a. The magnet subsystem consists of a stack of four 7.62 cm diameter by 1.27 cm thick disc NdFeB magnets. The RF source is a 7 cm diameter butterfly coil

consisting of 7 turns of #26 Cu wire in a 2 mm thick Teflon form. A capacitance of 34 pF gives ν_o = 14.5. MHz. The thickness of the RF coil and associated ground plane sets the minimum imaging depth of 2 mm. B_o and B_1 field performance were measured.[5] Three-dimensional magnitude and vector maps of the B_o and B_1 fields have been generated and meet our imaging requirements for perpendicularity. An NMR spectrometer located at RIT (referred to as the host) provides the RF power source; pulse sequencing programming environment; signal detection, digitization, and processing circuitry; and file storage system.

To pursue our research to the next level of capability, we were interested in locating a host that would provide us with higher RF power and faster signal sampling. Earlier, we determined that a NMR instrument equipped for solids analysis would give us an order of magnitude improvement in available RF power while also providing a 3x faster digitizer. An instrument that met all of our requirements was found at the research laboratories within Xerox Corp. (Webster, New York). After some discussions with 2 physicists who are responsible for all the spectrometers located at this plant, it became clear that a face to face meeting was necessary. In late February, Dr. Sam Kaplan and Dr. Alex Klymachyov visited R.I.T. to see our laboratory and to take a closer look at our *proof-of-concept* device. At the conclusion of this meeting, it was decided that our device posed no harm to their 400 MHz solids spectrometer, and that a schedule for access to this host could be worked out.

Experimental Part 1. Fabrication of Imaging Test Phantoms

In preparation for using this new host-instrument, several tasks were completed as outlined in the project plan section of the research proposal. The first task identified the need for new test targets that would work with our proof-of-concept device. As a result, several new test phantoms were designed and built. One phantom was designed specifically for testing depth performance within our device, while other radially non-symmetric phantoms were needed to further our understanding of the device's imaging performance. The depth-specific phantom design was based on the principles of the conic-section, whereby selecting a specific imaging depth would excite a particular diameter swath (spherical cap) with in this cone. The estimated diameter of the rendered image could be used to corroborate the estimated depth of operation for the device. The other 2 phantom designs were specifically designed to be radially non-symmetric while exploiting relatively easy to machine (i.e. milling tool) geometries. One target was designed to maximize the volume of the signal bearing material, thus maximizing the signal that could be acquired with our device. The last phantom design was more elaborate in its geometry while simultaneously optimizing the volume of the signal bearing material. All 3 phantoms designs have been fabricated using a non-signal bearing material (Teflon). Data collected from these targets will be shared in the Results sections of this report. See Appendix A. for details on the design and specifications for these 3 new phantoms.

Experimental Part 2. Acquisition Optimization with 100 W (legacy) host

Further work was completed using our legacy host system with the δ-version[6] of our RF coil. The goal of this work was to maximize depth penetration in preparation for work at the new host site. These tasks included:

1.) Re-optimizing the pulse sequence with the RIT host RF power amplifier limitations and

2.) Reacquiring the signal and full image sets of several phantoms at one depth on our 300 MHz host (RIT)

For the first task, a top-hat phantom (See Fig. 2.0) was used as the target and was filled with consumer-grade white petroleum jelly (Wegman's Brand, Rochester, NY). The phantom was placed on top and in contact with the δ-version[6] RF surface-coil and placed inside a Faraday chamber (See Fig. 3.0). The chamber's main function is to reduce environmental noise contamination from man-made sources. The air gap between the bottom surface of the coil (ground plane) and the top of the static magnet (B_o) was set to 8mm. Connectivity of our inductively coupled device and the host spectrometer was accomplished with a BNC connector. A direct X-channel connection between our device and the host was accomplished by by-passing the secondary prefilter of the QNP control module (floor). In this configuration, our device behaves like a passive NMR probe housed inside the bore of the spectrometer instrument. Impedance match of our device was measured and found to be close to 50 ohms as required by the host. The Q of the device was measured and found to be roughly 27 at its resonance frequency of 12.4 MHz.

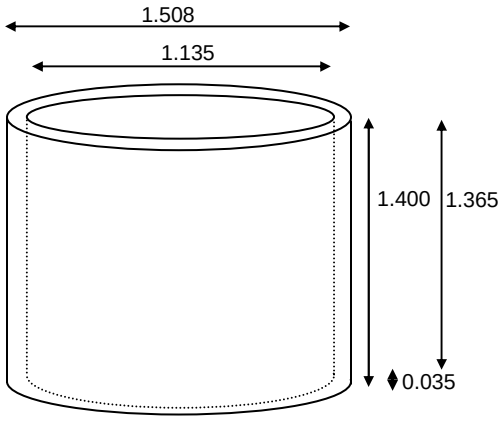

Figure 2.0 Basic Top-hat Phantom Target. The void volume can be filled with any signal bearing substance.

The design of the single-sided coil used on our *proof-of-concept* device is similar to that used in a transmit/receive antenna. Using our RF coil in transmit mode, a spin-echo RF-pulse sequence[10] is used to excite hydrogen proton spins along the resonant arc shown in Fig. 1b. The parameters that fully describe this pulse sequence are the repetition time (TR), the echo time (TE), and the applied static magnetic field. Four properties of the spin-bearing material also have an impact on the NMR signal magnitude. These properties include, sample temperature (T), spin density (ρ), spin-spin relaxation (T_2), and spin-lattice relaxation (T_1). The relaxation properties of the

petroluem jelly material were measured with the 300 MHz Bruker DRX spectrometer and were estimated as 216 ms and 160 ms for T_1 and T_2 respectively. To account for the static field gradient of our magnet system, TE was set to roughly T_2 /100, or 2 ms. TR was set equal to 5 times T_1 (set to ~1 second) for all experimental acquisitions. For all experiments, the sample temperature and pressure were held constant at standard conditions. The spin density of the petroleum material was not a variable in our testing and was assumed to be constant.

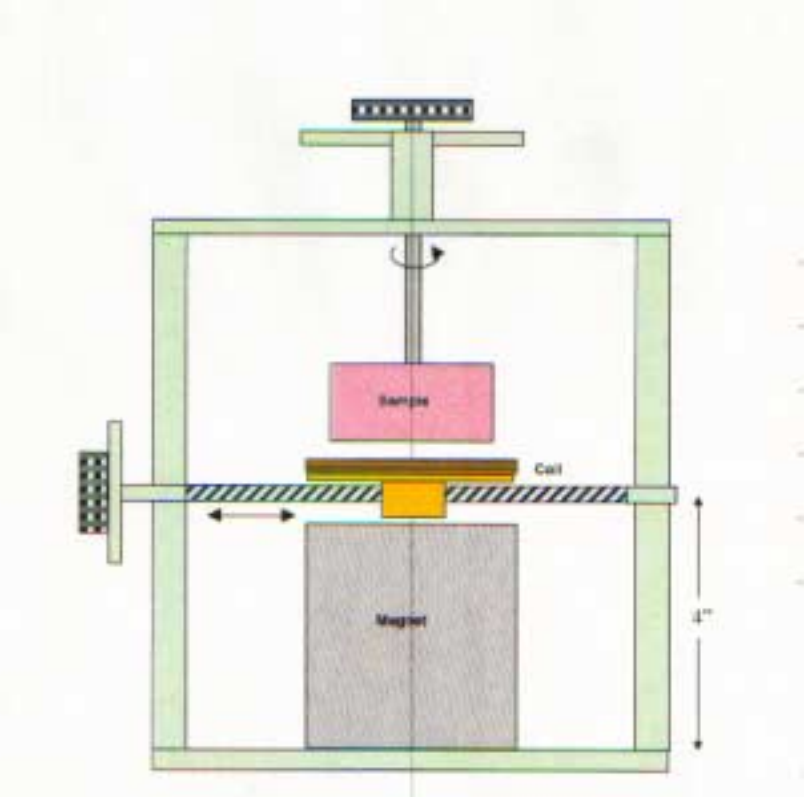

Figure 3.0 Faraday cage cross-section. The translation-arm is shown in between the coil and the static magnets. The rotational arm is shown attached to the sample.

During imaging acquisition, we fixed the sampling dwell time to 3.35 ms and the number of ensemble averages to 512 samples (for signal to noise improvement). Additionally, the spin-echo pulse program requires that the 90^o and 180^o RF pulses be fully specified. The parameters that control the pulse description include, the pulse shape, the pulse width (μs), and the power attenuation (dB). These pulse descriptors were experimentally varied and the signal intensity was measured for each case. Two RF pulse shapes (Sinc3[11] and Gaussian) were selected based primarily on 2 characteristics, a limited support in both time and frequency domains, and phase preservation within those domains. In our experimental design, Power attenuation was varied from –6 dB to over 40 dB (depending on available signal) for 3 pulse widths of 50, 200 and 800 μs for each pulse shape.

Detection of the signal is achieved by switching our RF coil to receive mode. Recall that an NMR signal generated from the relaxation of exited protons (FID), is a direct consequence of our spin-echo pulse sequence, and its governing parameters. The detected signal is amplified, digitized (Dwell time was fixed to 3.35 ms), averaged (512 realizations), and recorded by the host system. At each pulse program condition, the relative signal intensity was determined. This intensity value was determined from the peak of the calculated magnitude of the complex time-

domain free induction decay (FID) signal. The maximum amplitude observed at a given power attenuation and pulse width would correspond to the optimum condition for the $90^{o}/180^{o}$ rotation needed for the spin echo sequence.

Imaging parameters optimized in the fashion just described were used to acquire intensity data making up several projections from our newly fabricated phantoms. A Faraday cage equipped with the translation arm and the rotation dial were used in all imaging experiments. See Figure 3.0 for details on the Faraday cage. The non-radially symmetric phantoms were scanned with acquisition parameters outlined above. Five projections of the "Quad slot" phantom were recorded with a sampling pitch of ~0.055 inches. A total of 28 samples were acquired for each projection. Five different projection angles were acquired at 0, 30, 45, 60, and 90 degrees relative to a arbitrary datum established mechanically on the external surface of the phantom.

The experimentally produced projection points were computed using 9 points extracted from the signal. A simple 5-point triangular windowing technique was used to smooth the magnitude data. After the filtering of these nine values, the intensity value representing the peak was recorded as a function of position for the final projection plot. The experimentally acquired projection was compared to an "ideal" projection created using a computer model. The plots of these comparisons are shown in the Results section of this report.

Similar scans of the "Off-center Cylinder" phantom were captured. The projection angles acquired for this target were 0, 30, 60 and 90 degrees, respectively. The results obtained from this phantom were comparatively similar to those obtained from the more complicated (*i.e.* Quad-slot) phantom discussed above. The particular results obtained from the latter phantom have been omitted from this report to improve clarity.

Experimental Part 3. Acquisition with 1000 W host

With help of Dr. Sam Kaplan and Dr. Alex Klymachyov at the Xerox research labs, the initial set-up with the 400 MHz instrument was fairly straight forward. The acquisition parameters and the pulse program were downloaded over the internet through FTP. The pulse program needed a common **#include** file appended at the top of the code in order to work properly within the newer acquisition environment. The Gaussian pulse was modified to account for their newer software environment (**xwinnmr** V 3.6 Linex OS) and the faster digitizer. One thousand points were used to create the Gaussian-shaped pulse using the shape tool provided with **xwinnmr**. A ^{103}Rh (12.594148 MHz) nucleus was used to get close to the target resonant frequency of 12.4 MHz.

Our passive probe system was connected to the 400 MHz host system in a similar fashion used before with the legacy host (*i.e.* 8mm spacing). The target used for a proton source was the petroleum jelly filled top hat phantom used in prior experiments. The 400 MHz Cryo-magnet was by-passed at the secondary prefilter of the QNP control module located on the floor near the base of the instrument. Because this was a solid-state spectrometer, there were several more prefilter modules as compared to the legacy spectrometer. The prefilter module used was labeled as "X-channel High Power", which was also rated at 12-32 MHz. A direct BNC connection from this module was tied into a Bi-directional Co-axial coupler (rated 50-1000 MHz) for

simultaneous interrogation of the RF signal going into our probe as well as interrogation of the reflected signal. Our "*proof of concept*" probe was connected to one end of the coupler and a 45 dB attenuated LeCroy 9354A 500 MHz Oscilloscope was connected to the other end. No external attenuation was used with our probe.

The power attenuation needed with the new system to match the attenuation used with the legacy system was determined to be 11 dB and 8 dB for the 90 and the 180 (actually 127.43) degree pulses, respectively. The acquisition parameters that were used to control the 90 and the 180 degree attenuation were SP2 and SP3, respectively. Initially, the attenuation was set to a "safe" level of 13 and 10 dB respectively. A short acquisition experiment was run to ascertain proper performance. The RG parameter was adjusted manually at first and then an internal program was run to determine the gain through a recursive algorithm imbedded in **xwinnmr**. The final gain factor used was ~16K (16,384) for all subsequent acquisitions. Within the acquisition parameters, DE was increased to 20 μs to get rid of the ring-down residual signal from the host amplifier. The DW parameter was initially set to 3.35 μs to match what was used with our legacy experiments.

A small series of approximately nine experiments were run to converge on the proper power attenuation for the optimal $90^o/180^o$ RF pulses. The attenuation was varied from 11, 8 dB to 15, 12 dB at 0.5 dB increments. The data was recorded and saved in separate files. Magnitude calculations of the complex echo signal were used to estimate the signal intensity in the time domain. The intensity magnitude was recorded.

For next series of experiments, several changes were made in the acquisition parameters in order to achieve faster acquisition performance with minimal impact on signal amplitude. The following acquisition parameters were changed to the following settings; TR = 0.2 sec, DW = 1.333ms, TD = 1K, and NS = 1000. A 0.125" thick spacer was placed on the bottom of the static magnet causing the air gap to be reduced from 8mm to 4.825 mm. (See Figure 3.0 for details.) The $90^o/180^o$ pulse difference was increased from 3 dB to 6 dB to increase the acquired signal amplitude. The SP2 and SP3 parameters were varied from 9 and 3 dB to 20 and 14 dB, respectively using 1dB increments. The results of each acquisition were recorded and saved in individual files. An auxiliary program called **TopSpin** was used to compare the signal intensities (i.e. magnitude) for these experiments.

Results and Discussion

The results obtained using the procedure outline in the Experimental Part 2.0 section is shown in the following two figures. Acquisition optimization with two well behaved RF pulse shapes was completed at close to 100 W with the Sinc3 and the Gauss respectively. The Gauss shaped pulse data is shown in figure 4.0. The data obtained with the Gauss shaped pulse proved

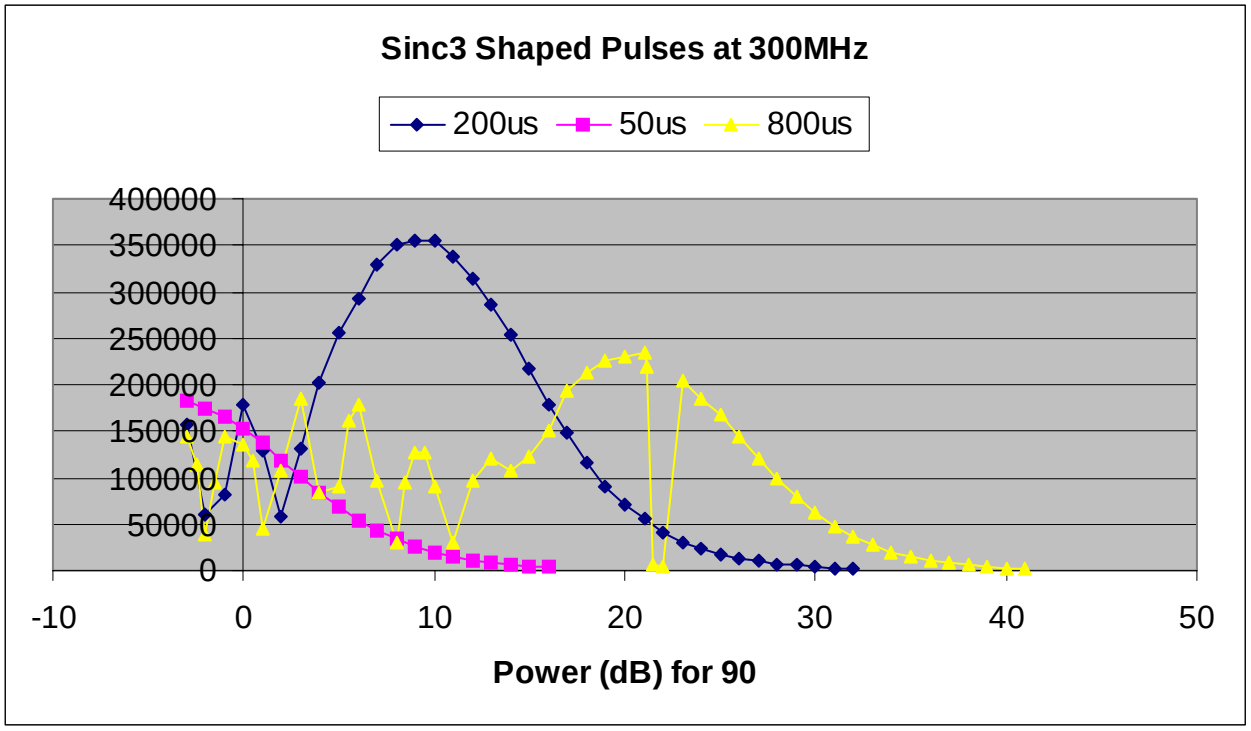

Figure 4.0 RF Pulse optimization with the Sinc3 shaped pulse at ~100 Watts

to be better behaved over a larger power range for the three pulse widths studied. The shortest pulse width (50 μs) was selected by direct application of the similarity theorem[12] of Fourier transform pairs. The intent is to excite the broadest (i.e. maximize the Thk parameter) swath through our proton rich material held within the void of our top-hat phantom. The experiment was re-run with finer sampling using the 50 μs width Gaussion pulse. The largest signal was found using –1.5 and –4.5 dB for the 90^{o} and the 180^{o} respectively. Equipped with these pulse width and pulse shape results, we proceeded on with the next step of imaging.

Imaging with our newly fabricated non-radially symmetric phantoms (See Appendix A. for phantom descriptions) was accomplished using the procedure outlined in the Experimental Part 2.0 section of this report. Five projections obtained from the Quad. Slot phantom have been included in this report (See Figs. 5-9). The off-axis cylinder phantom data has been omitted as the results were similar to those reported with the Quad. Slot phantom. Figures 5-9 compare the ideal projection and its experimental counterpart for 5 different angles ranging from 0 to 90 degrees. The agreement was found to be acceptable and no further image processing was done.

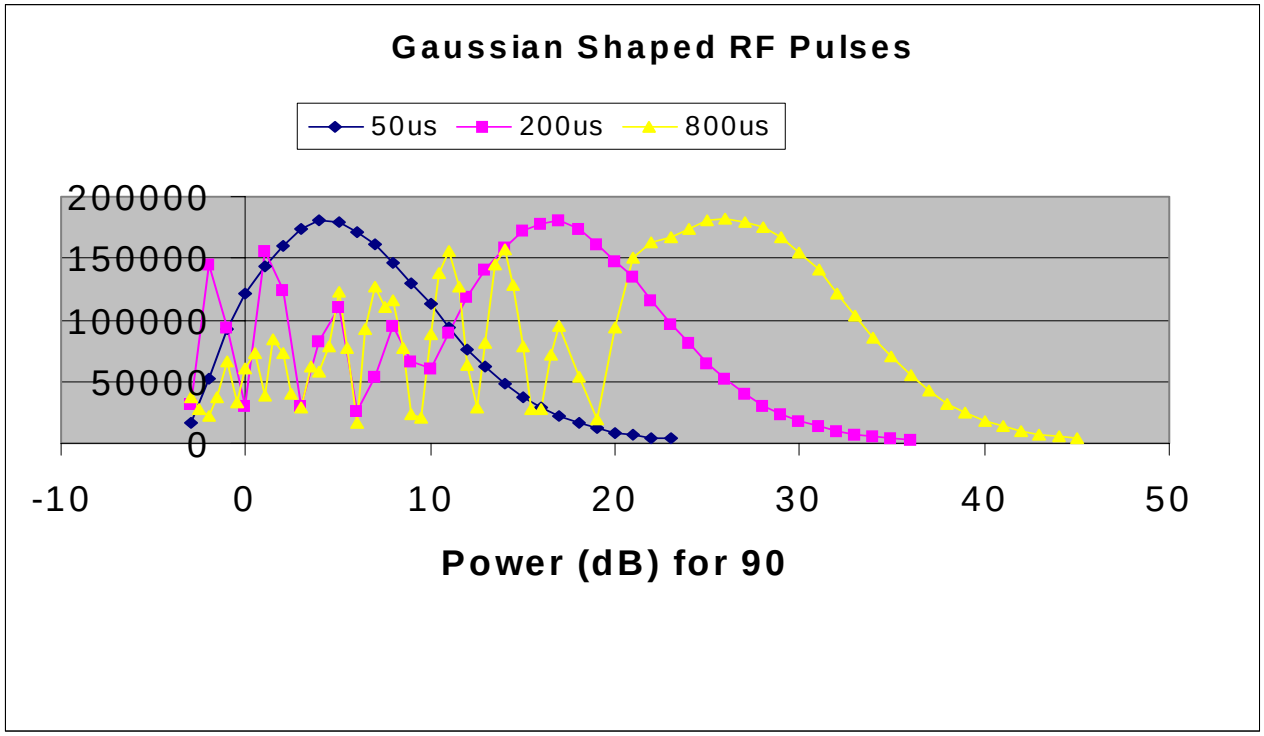

Figure 5.0 RF Pulse optimization with the Sinc3 shaped pulse at ~100 Watts

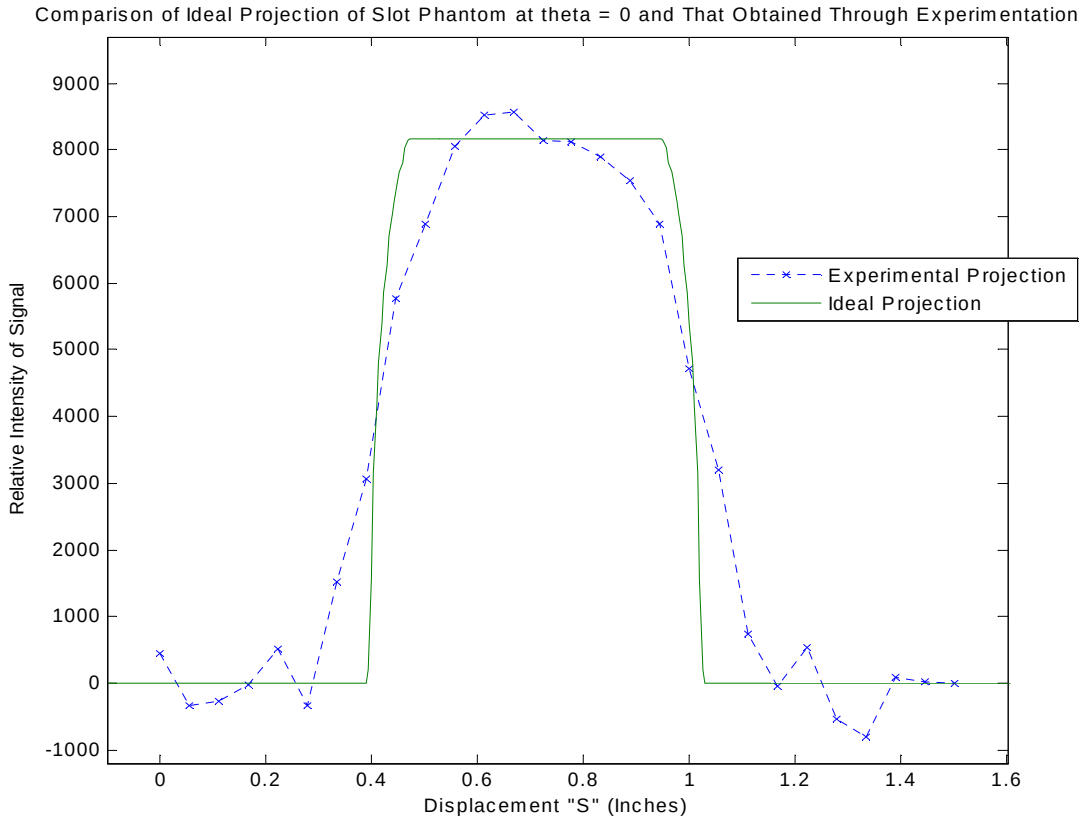

Figure 6.0 The reference projection for the Quad. Slot phantom at roughly 0^{o}.

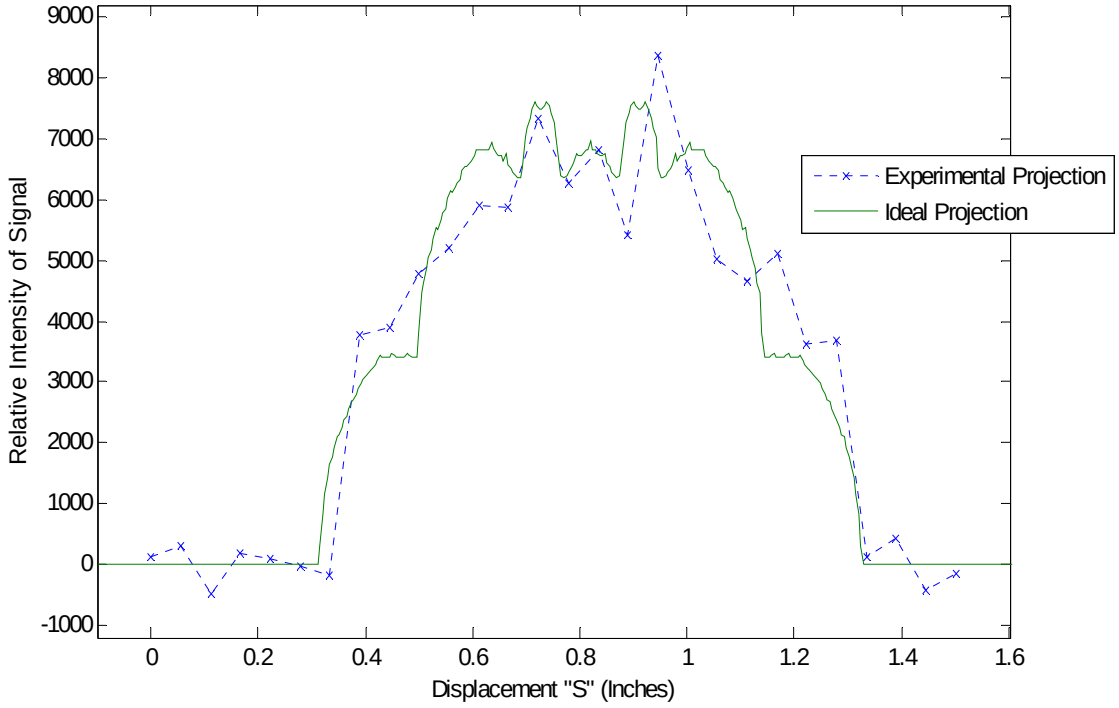

Figure 7.0 Comparison of experimental data and ideal for Quad Slot phantom at 45°.

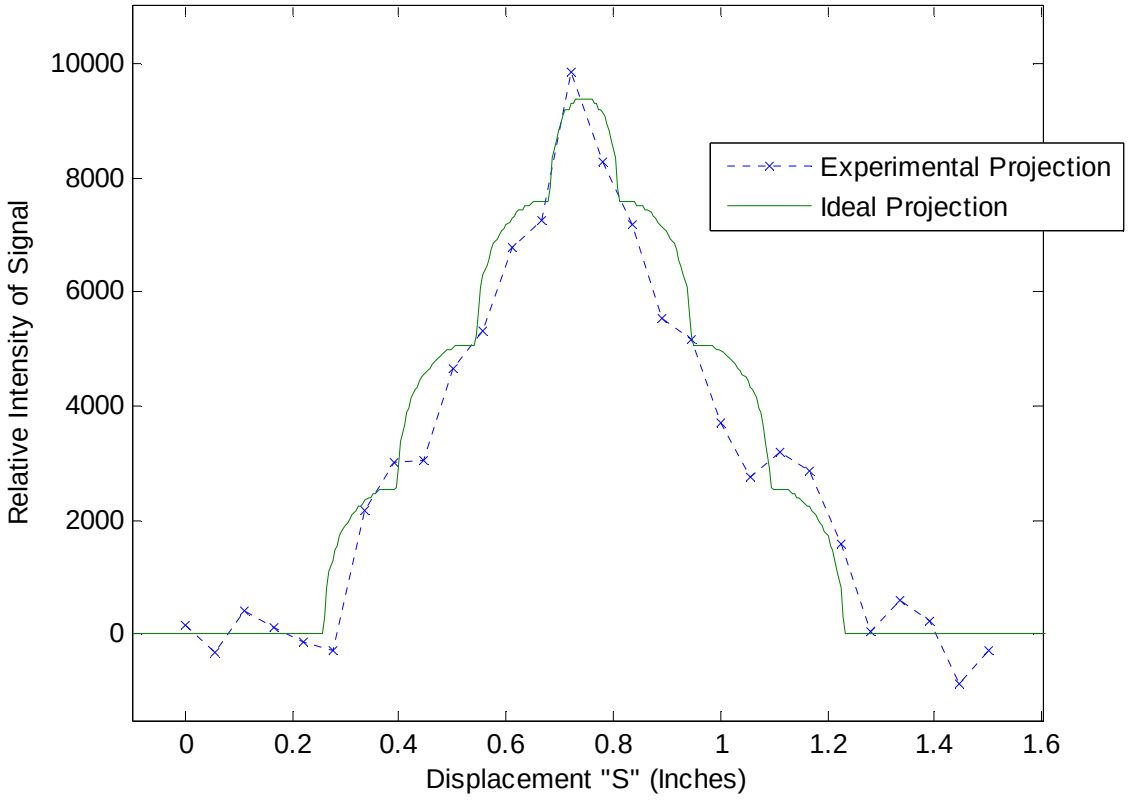

Figure 8.0 Comparison of experimental and ideal projection data for the Quad. Slot phantom at 30°.

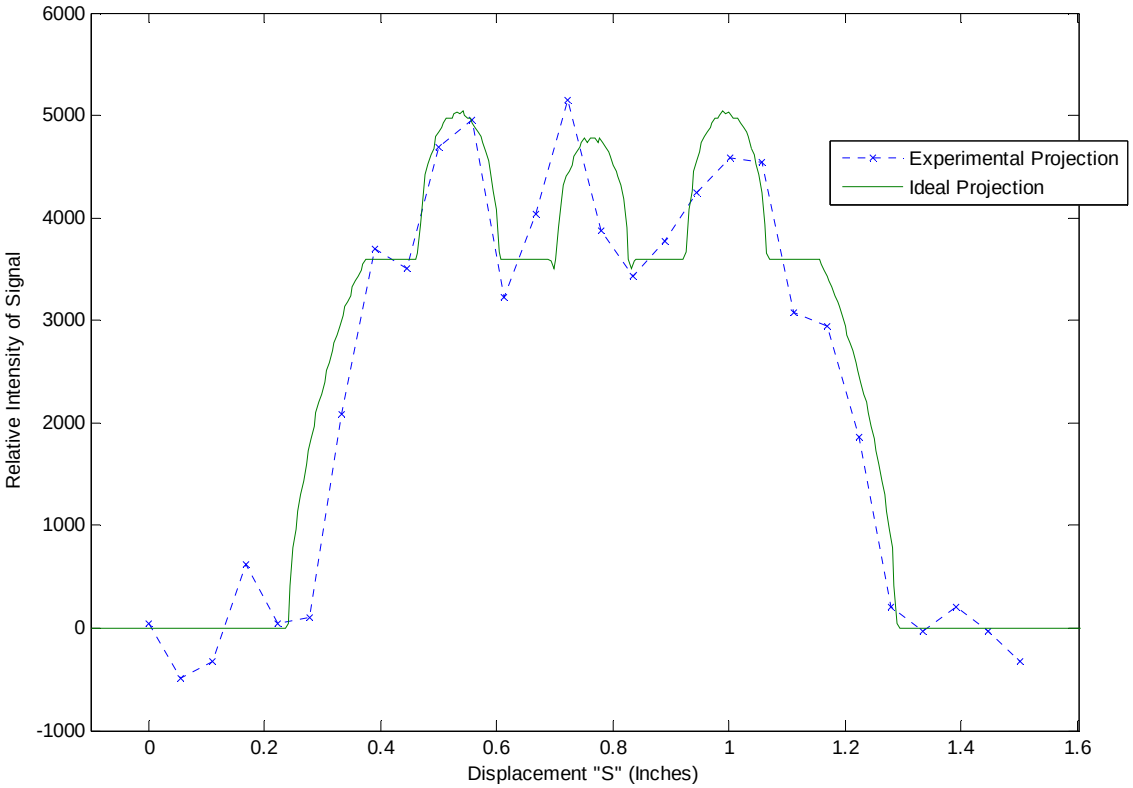

Figure 9.0 Comparison of experimental and ideal projection data for the Quad. Slot phantom at 60^{o}

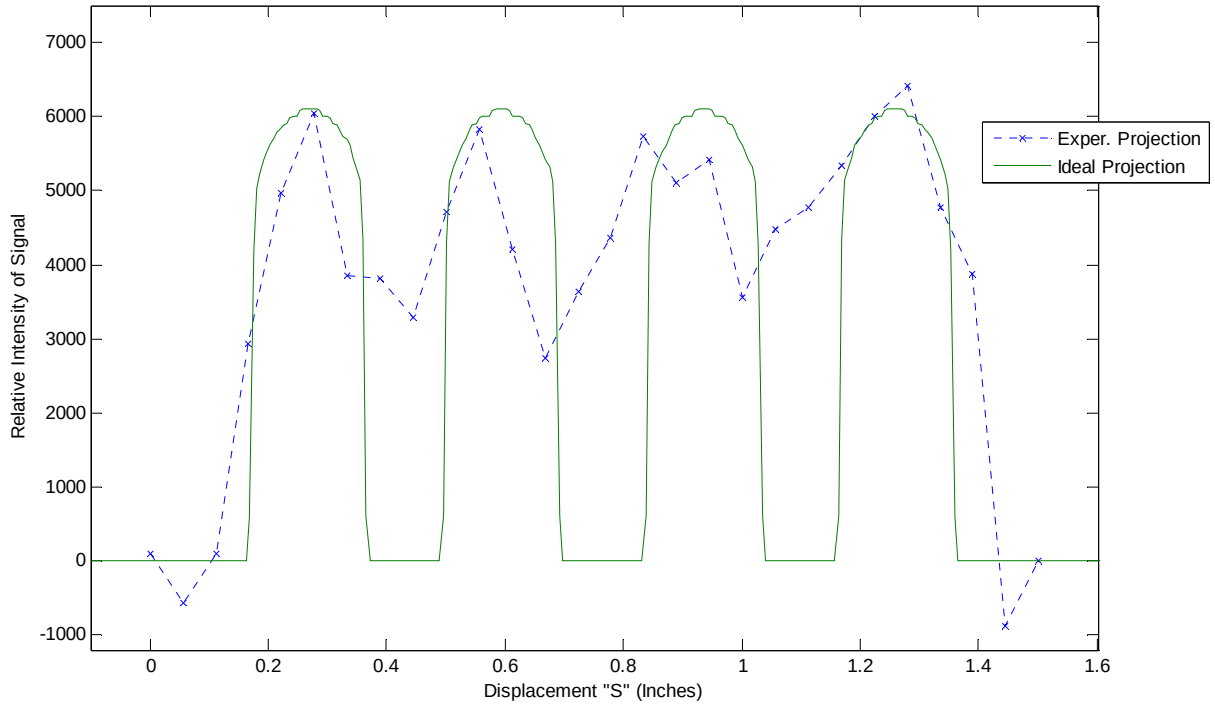

Figure 10.0 Comparison of experimental and ideal projection data for the Quad. Slot phantom at 90^{o}

The results achieved with our local host system established a lower bound on the imaging parameters and set expectations for image signal quality at the most shallow depth setting. These imaging parameters were uploaded to the 400 MHz, solids equipped Bruker spectrometer and installed as a new experiment file on this host system.

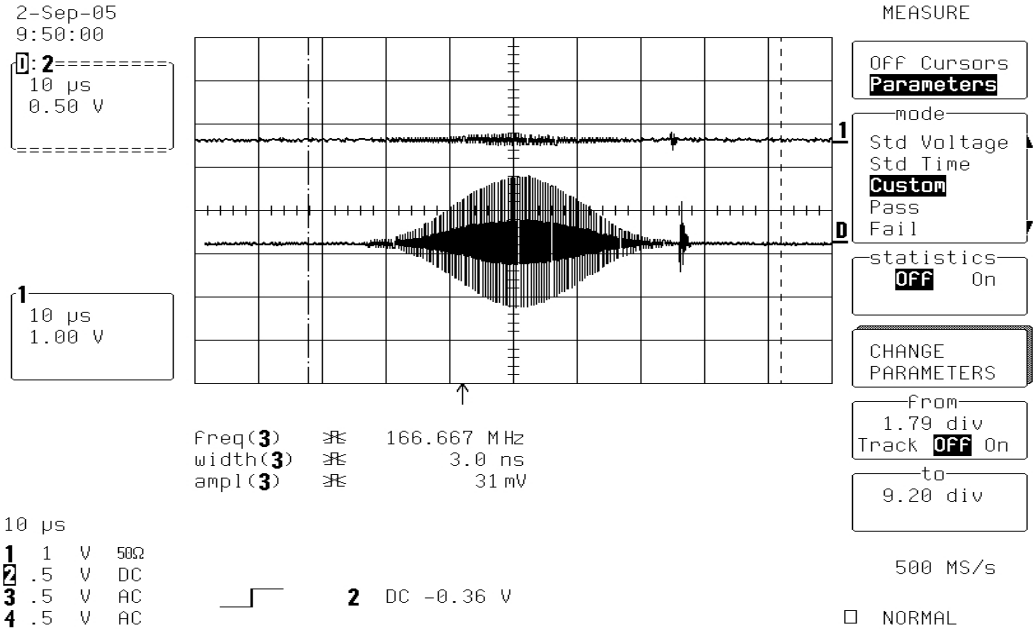

Figure 11. Oscilloscope traces for the Gaussian RF pulse. The top trace corresponds to the reflected (energy not properly absorbed) signal. The Bottom trace corresponds to the forward (input) signal.

On the 400 MHz system, the Gaussion RF pulses (See Fig. 11.0) used in our spin echo sequence was continuously monitored in both forward and reflected modes. Slight ringing was observed trailing the RF signals. These were reduced to an acceptable level by varying the delay (D30) used before the start of the Acquisition cycle within the Receiver module (See Fig. 12.0).

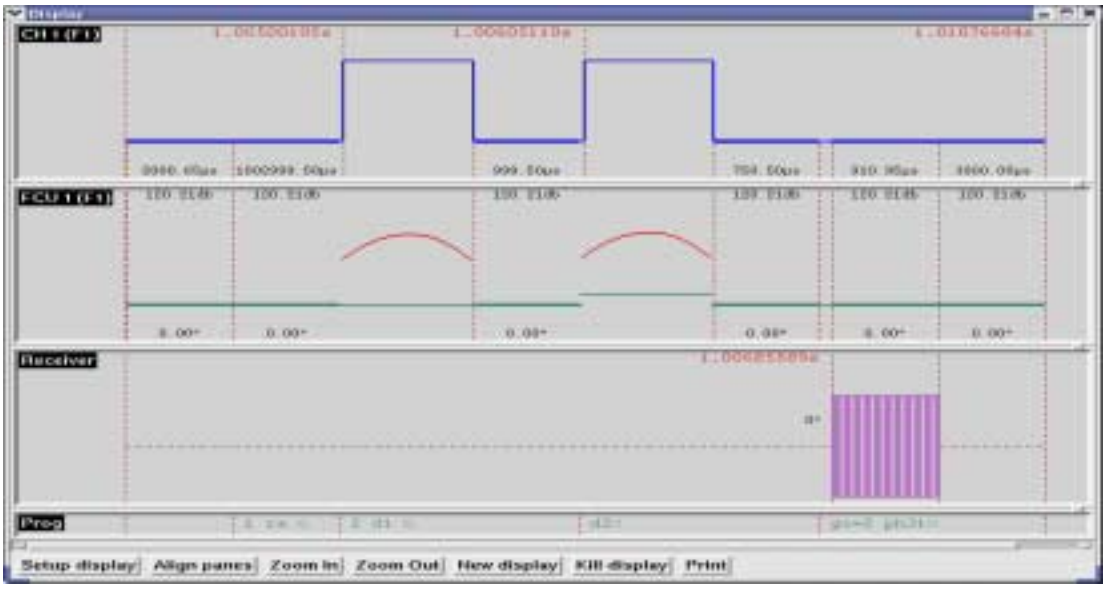

Figure 12. Screen capture of the spin echo pulse program for one cycle using the **plusdisp** utility within **xwinnmr**. The pulse width, power, and shape parameters as well as delay times are shown.

The first experiment done with the new host was to establish similar operating conditions estiblished with the 300 MHz host. Given our first estimate on the power attenuation to be roughly 100 Watts with the legacy host system, it was determined that we needed roughly 11 and 8 dB to match our power requirements for the 90^{o} and the 180^{o} on the 400 MHz system. To verify that we had the correct attenuation settings, a series of experiments were run over night. In these series of experiments, the attenuation was varied from 11, 8 dB to 15, 12 dB at an increment of 0.5 dB. The results of these runs are plotted in Figure 13.0.

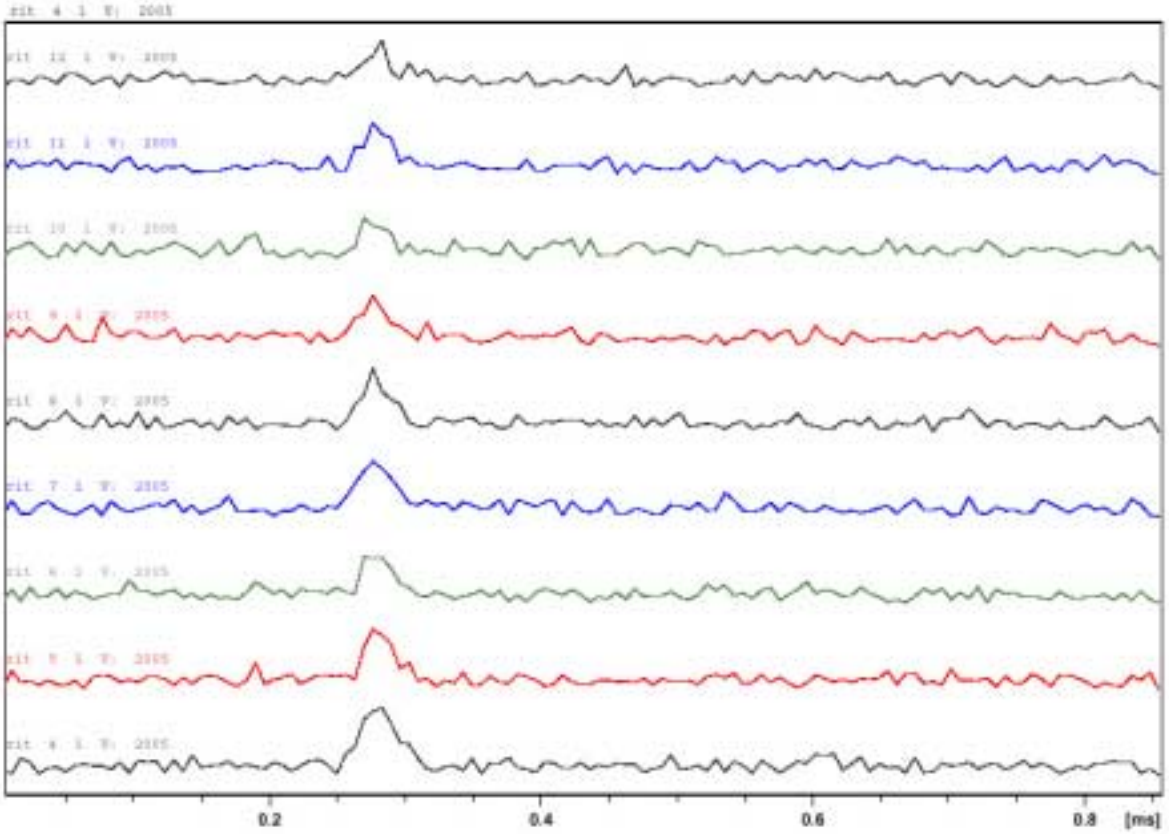

Figure 13.0 Power Attenuation series with the 400 MHz system. Our *Proof-of-concept* probe was used with the top hat phantom filled with petroleum jelly. Resonance was established at 12.45 MHz. Trace Exp # 4 corresponds to 11, 8 dB attenuation with increasing attenuation up to 15, 12 dB shown in trace Exp #12.

As described in the experimental sections of this report, the echo signal acquired was post processed using the **mc** command within **xwinnmr**. This command performs a magnitude calculation on the complex time-domain echo signal. This magnitude or *intensity* signal was plotted in sequential fashion for quick and easy comparisons. It was clear that the signal amplitude and the signal width was decreasing with decreasing power. Based visual data analysis using the graph generated with **TopSpin** software (See Fig. 13.0), we were easily convinced that the lower bound estimate of 11 and 8 dB would be a sufficient starting point for further experiments. Given more time on the instrument, more testing would have been done to probe lower attenuation settings to verify that indeed the largest signal amplitude was captured.

Armed with ~ optimal acquisition parameters, we proceeded on with the depth experiments. The *proof-of-concept* probe was modified by adding a 0.125" circular spacer between the static magnet stack and its base support (See Fig. 3.0 for details). The addition of this spacer resulted in an increase of roughly 3.18 mm of depth into the top hat phantom. Based on educated intuition, we assumed that more power would be required to excite the resonant swath which was 3.18 mm further away from the coil as compared to our prior experimental set up. Based on this assumption, a series of experiments were designed that varied

power attenuation over a larger, more energetic range of RF pulses. Concurrently, the power range was adjusted to more accurately mimic the 90^o and 180^o pulses required to get better rotational performance with our probe. This change required that the difference between the 90^o and the 180^o RF pulse be 6 dB. With this in mind, a 15 experiment series was coded up that varied power attenuation from {6 and 0 dB} to {20 and 14 dB} with a 1.0 dB increment between experiments. The series of experiments were run over night taking roughly 14 hours of instrument time to complete.

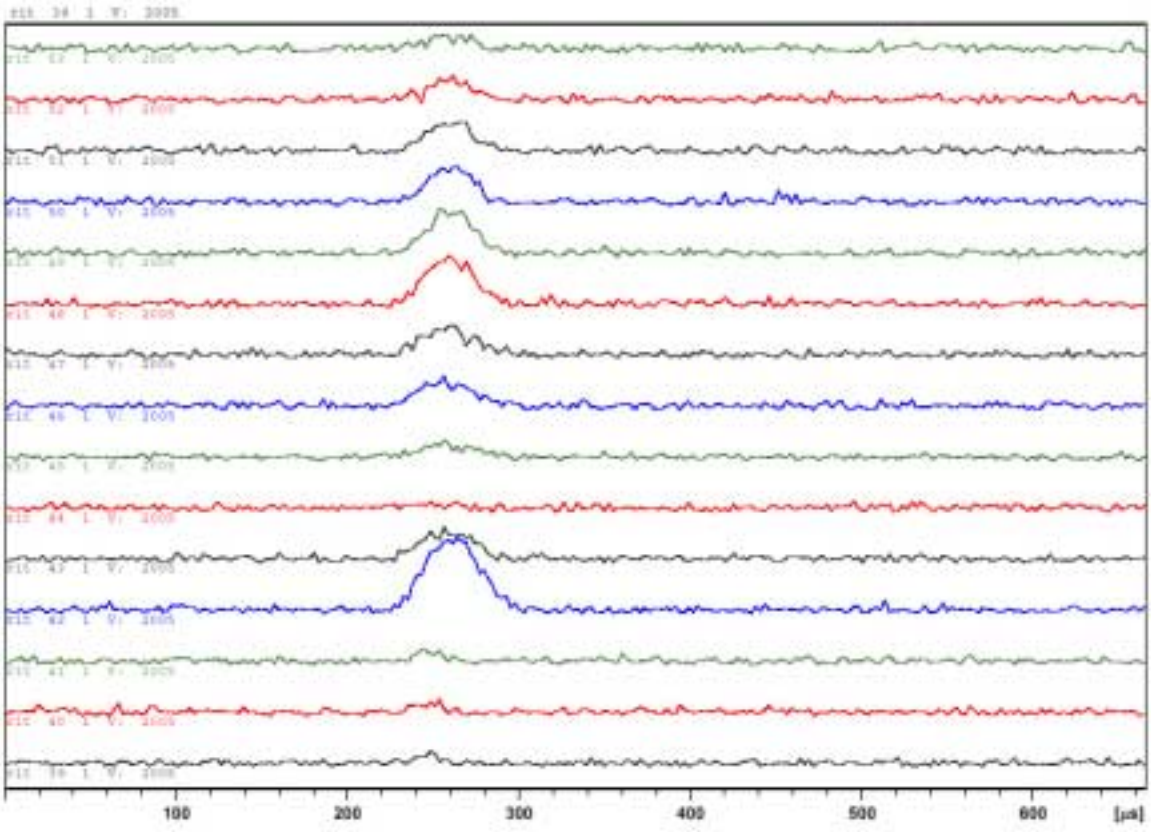

Figure 14.0 Power Attenuation series with the 400 MHz system. Our *Proof-of-concept* probe was used with the top hat phantom filled with petroleum jelly configured at an additional target depth of 3.18 mm. Resonance was established at 12.45 MHz. Trace Exp # 39 corresponds to {6 and 0 dB} attenuation with increasing attenuation up to {20, 14 dB} shown in trace Exp #53.

The complex echo data collected with these 15 or so experiments were processed via the **mc** command and sequentially plotted via **TopSpin** software as discussed previously. The processed results are illustrated in Figure 14.0. The sequence shows some interesting trends as observed looking at the top trace that correspond to less power, and progressing down the figure to traces obtained from increasingly higher power. Initially the trend observed with the data was well behaved and met our expectations. However, between experiment number 48 and 47 the signal intensity was found to be decreasing. The signal continues to decrease monotonically until experiment number 43 through 42. In this portion of the experiment, the intensity was observed to increase very quickly. Two maximums observed within our experimental series was not expected. Further investigation of the *proof-of-concept* probe and its signal integrity was prompted. Analysis of the input and the reflected RF pulse traces via the LeCroy Oscilloscope from the host and our probe gave a glimmer of insight. At higher power, it was clear that our probe was experiencing some electrical arching. Given our fast cycling times and our relatively small duty cycle, visual observation of the arching phenomena was not possible. Some simple changes to the pulse with and the TR time, we could visually confirm the electrical arching and pin point its prominent

location within the surface coil windings. Four layers of Teflon tape were used to try to better insolate the windings from the ground plane where the prominent arching was occurring. This small change within the surface coil windings gave little improvement with respect to the arching. Based upon empirical calculations, it was determine that our surface coil started to arch at approximately 178 Watts. This is roughly two times the available power on our legacy host spectrometer.

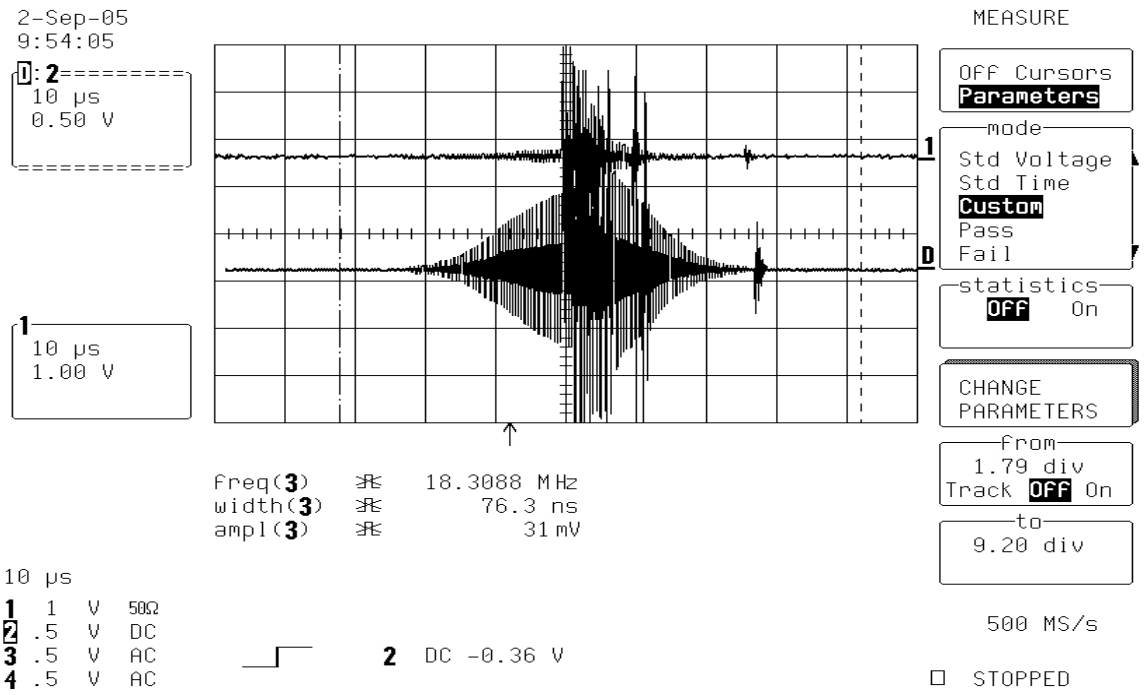

Figure 15.0 Oscilloscope traces obtained from the proof-of-concept probe operating at 12.45 MHz using a petroleum jelly filled top hat phantom. The input Gaussian RF pulse is attenuated at the level of 6 on a 400 MHz, 1000W solid state Bruker spectrometer. The reflected trace is shown on top.

Going back to the oscilloscope, we were able to confirm the electrical arching effects on the RF pulse signal integrity. The arching affect on our coil's RF signal was rather dramatic and is shown in Figure 15.0. Given the state of our probe, it was determined that further depth experimentation would not be useful.

Conclusions and Further Work

A *proof-of-concept* probe resonating at 12.45 MHz was tested with a legacy 300 MHz host spectrometer. The probe was configured with a petroleum jelly filled top hat phantom with a minimal depth of penetration established by an 8mm air gap between the coil and the top of the static magnet. Signal acquisition parameters were optimized for a spin echo sequence and several projections were subsequently acquired from 2 non-radially symmetric phantom targets. Acceptable imaging performance was obtained with the probe in this setting, operating with its optimized acquisition parameters.

A 400 MHz solid state capable spectrometer was found that met our power requirements and several days of instrument time was obtained. Baseline operating conditions established with the legacy instrument were duplicated on the 400 MHz host with our *proof-of-concept* probe. Depth experiments using the new host were started giving early results that indicated that our coil windings needed some additional insulation. It was clear that the new host had excess power capacity to achieve penetration depths of approximately 1 cm. Future work will include using higher gauge copper wire with better insulation with our current δ-coil geometry.

The experience working with Dr. Kaplan and Dr. Klymachyov at Xerox Research Labs was invaluable. Many different nuances about the **xwinnmr** program and its numerous utilities were shared as well as several time saving rules of thumb in the area of multiple signal acquisition experiments. It was a very satisfying experience for everyone involved with the depth experiments associated with our *proof-of-concept* probe. The Xerox researchers expressed an interest to continue working with us on this project. Based on these conversations, further collaboration with Xerox is expected to continue when we have implemented our improved coil design for our single-sided imaging probe.

At this time, we are exploring the merits of presenting these results at multiple venues. Under consideration is the ISMRM meeting in Seattle WA., May 2006, or the SAGEEP[13] meeting in Seattle WA., April 2006, as well as publishing in a peer reviewed journal.

References

1. L. B. Conyers, Ground Penetrating Radar, 463-476, ed. J.P. Hornak, *Encyclopedia of Imaging Science and Technology*, John Wiley & Sons (2002)
2. C. L. Bray, *et al*., An R_1 & R_2 Distribution Study of Hydrated Randomly Close Packed Synthetic Soils, 15th ISMAR, Point Verda Beach, FL, October 2004.
3. C. L. Bray, *et al*., An R_1 Distribution Study of Hydrated Randomly Close Packed Synthetic Soils, 45th ENC, Asilomar, CA, April 2004.
4. M. Bostick, *et al.*, An NMR Relaxation Rate Study of Hydrated Randomly Close Packed Synthetic Soils. 32nd Northeast Regional Meeting of the American Chemical Society. Rochester, NY, November 2004.
5. C. L. Bray, *et al*., Design and Characterization of a Sub-Surface MRI System, 15th ISMAR, Point Verda Beach, FL, October 2004.
6. C. L. Bray, *et al*., Design Iterations and Performance Enhancement for a Sub-Surface MRI System, *(Submitted)* 46th ENC, Providence RI, April 2005.
7. T. Munsat, W. M. Hooke, S. P. Bozeman, S. Washburnd, Two new planar coil designs for a high pressure radio frequency plasma source. *Appl. Phys. Lett.* **66** :2180-2182 (1995).
8. P.G. Lauterbur, Image formation by induced local interactions. Examples employing NMR. *Nature* **242:**190-191 (1973).
9. S. R. Deans, *The Radon Transform and Some of its Applications*, Appendix A., Krieger Pulishing Company, Florida, 204-217 (1993).
10. J. P. Hornak, *The Basics of MRI*, (http://www.cis.rit.edu/htbooks/nmr/) Interactive Learning Software, 2005.
11. Bruker **xwinnmr** V2.6 acquisition software manual, Bruker, Billerica, MA. 1997.
12. Bracewell, R.N., *The Fourier Transforms and its Applications*, Second Edition, Revised, McGraw-Hill Inc., 1986.
13. www.eegs.org/sageep/index.html

Appendix A.

Phantom Design Drawings and Schematics

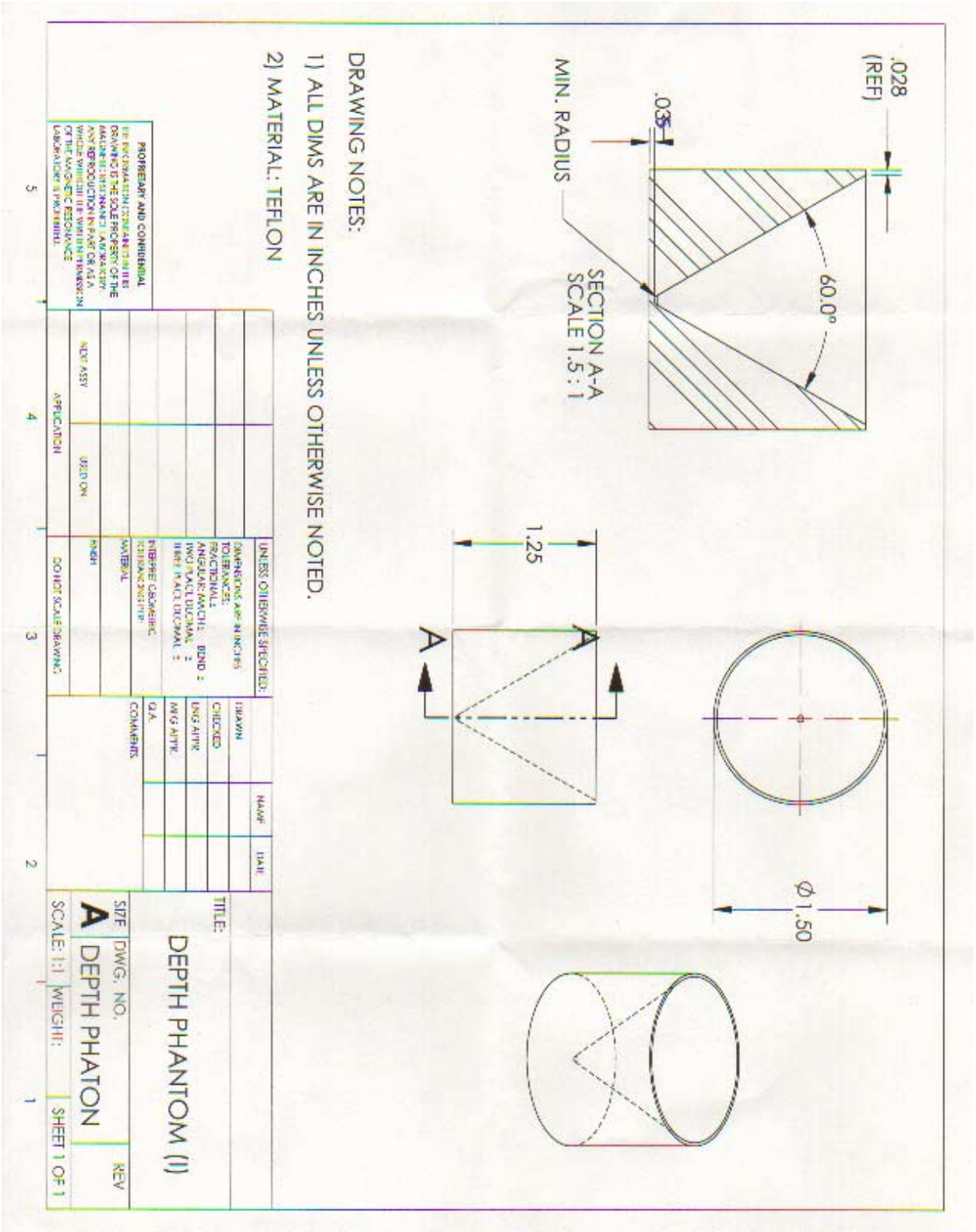

May 20, 2005

Tom and Donovan:

Here are sketches of 2 phantom designs that I am interested in working with. The first is a couple of simple off-center cylinders (See Fig. 1.0 for details). The dimensions provided are approximate only! The next phantom design is similar to a drawing all ready prepared by Donovan Adams.

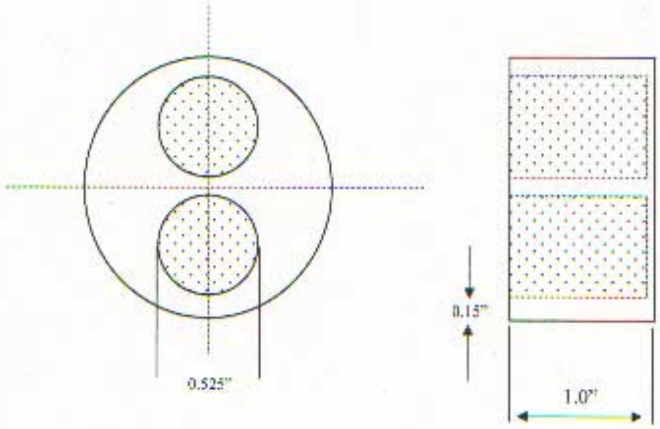

Figure 1.0: Double Cylinder Phantom for Imaging with Delta-2 at 12.45 MHz.

The next phantom (See Fig. 2.0) is more like the resolution phantom for which a technical drawing already exists (I have this on file). The purpose of this phantom is to stress smaller features while maintaining decent signal to noise (SNR) ratio. Spacing and feature size has been increased relative to the prior "Resoluton Phantom I" design. Please let me know how I can help with this. Thank you!

Tina Bray
Magnetic Laboratory
RIT

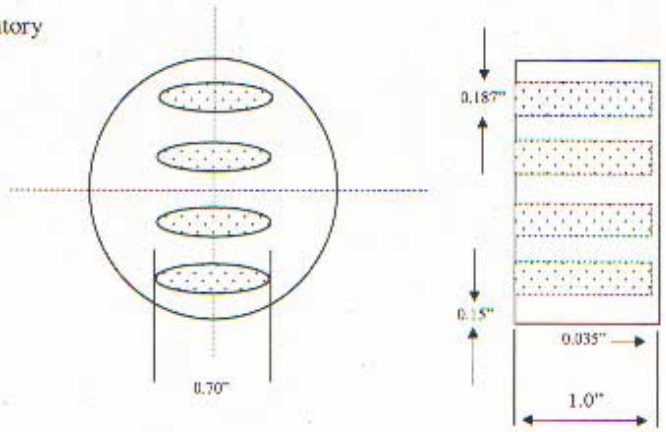

Figure 2.0: Quad of elongated cylinders resolution phantom for imaging with Delta-2 at 12.45 MHz.